BIOCHEMISTRY
including biophysical chemistry & molecular biology
Article

Biochemistry **2009,** *48,* 8879–8890 8879
DOI: 10.1021/bi901046x

The Mechanism of the Reaction Catalyzed by Uronate Isomerase Illustrates How an Isomerase May Have Evolved from a Hydrolase within the Amidohydrolase Superfamily†

Tinh T. Nguyen,§ Alexander A. Fedorov,‖ LaKenya Williams,§ Elena V. Fedorov,‖ Yingchun Li,§ Chengfu Xu,§ Steven C. Almo,*,‖ and Frank M. Raushel*,§

§*Department of Chemistry, P.O. Box 30012, Texas A&M University, College Station, Texas 77842-3012, and*
‖*Department of Biochemistry, Albert Einstein College of Medicine, 1300 Morris Park Avenue, Bronx, New York 10461*

Received June 20, 2009; Revised Manuscript Received August 10, 2009

ABSTRACT: Uronate isomerase (URI) catalyzes the reversible isomerization of D-glucuronate to D-fructuronate and of D-galacturonate to D-tagaturonate. URI is a member of the amidohydrolase superfamily (AHS), a highly divergent group of enzymes that catalyze primarily hydrolytic reactions. The chemical mechanism and active site structure of URI were investigated in an attempt to improve our understanding of how an active site template that apparently evolved to catalyze hydrolytic reactions has been reforged to catalyze an isomerization reaction. The pH−rate profiles for k_{cat} and k_{cat}/K_m for URI from *Escherichia coli* are bell-shaped and indicate that one group must be unprotonated and another residue must be protonated for catalytic activity. Primary isotope effects on the kinetic constants with [2-^{2}H]-D-glucuronate and the effects of changes in solvent viscosity are consistent with product release being the rate-limiting step. The X-ray structure of Bh0493, a URI from *Bacillus halodurans*, was determined in the presence of the substrate D-glucuronate. The bound complex showed that the mononuclear metal center in the active site is ligated to the C-6 carboxylate and the C-5 hydroxyl group of the substrate. This hydroxyl group is also hydrogen bonded to Asp-355 in the same orientation as the hydroxide or water is bound in those members of the AHS that catalyze hydrolytic reactions. In addition, the C-2 and C-3 hydroxyl groups of the substrate are hydrogen bonded to Arg-357 and the carbonyl group at C-1 is hydrogen bonded to Tyr-50. A chemical mechanism is proposed that utilizes a proton transfer from C-2 of D-glucuronate to C-1 that is initiated by the combined actions of Asp-355 from the end of β-strand 8 and the C-5 hydroxyl of the substrate that is bound to the metal ion. The formation of the proposed *cis*-enediol intermediate is further facilitated by the shuttling of the proton between the C-2 and C-1 oxygens by the conserved Tyr-50 and/or Arg-355.

Uronate isomerase (URI)[1] catalyzes the first step in the pathway for the metabolism of D-glucuronate and D-galacturonate. In this transformation, D-glucuronate and D-galacturonate are initially isomerized into their corresponding keto products, D-fructuronate and D-tagaturonate, respectively (*1*). D-Fructuronate and D-tagaturonate are then reduced to D-mannonate and D-altronate, respectively, by mannonate and altronate dehydrogenase in the presence of NADH (*2*). The pathways converge through a dehydration reaction in which mannonate dehydrase and altronate dehydrase convert mannonate and altronate to 2-keto-3-deoxy-D-gluconic acid (KDG). This product is then phosphorylated by the enzyme ketodeoxygluconic acid kinase with ATP to form 2-keto-3-deoxy-6-phosphogluconic acid (KDG-6-P). In the final step of this pathway, 2-keto-3-deoxy-6-phosphogluconic acid is cleaved by an aldolase to yield pyruvate and D-glyceraldehyde 3-phosphate, which enter the citric acid cycle and glycolysis. The entire pathway is summarized in Scheme 1 (*1*, *2*).

We have demonstrated that uronate isomerase is a member of the amidohydrolase superfamily of enzymes based on sequence alignments and three-dimensional structural comparisons (*3*). The majority of the functionally characterized members of the amidohydrolase superfamily catalyze the hydrolysis of amide or ester bonds to carbon or phosphorus centers (*4*, *5*). Well-characterized examples include dihydroorotase (*6*), urease (*7*), and phosphotriesterase (*8*). Members of this superfamily also catalyze the deamination of many nucleotides, including adenosine (*9*), cytosine (*10*), and guanine (*11*). The active sites of these enzymes generally contain a mononuclear or binuclear metal center that is perched at the C-terminal end of the β-barrel within a $(\beta/\alpha)_8$ structural fold. The most highly conserved residues in the AHS include two histidines from β-strand 1, histidines after the ends of β-stands 5 and 6, and an aspartic acid from β-strand 8. Since URI catalyzes an isomerization of an aldose sugar to the corresponding ketose product, this enzyme is one of the most divergent members of the amidohydrolase superfamily. The mechanistic details of this transformation are therefore of significant interest for an improved understanding of how an active site that originally evolved to catalyze hydrolytic reactions has been reforged to undergo an isomerization reaction.

†This work was supported in part by the National Institutes of Health (Grant GM71790) and the Robert A. Welch Foundation (A-840).

*To whom correspondence should be addressed. F.M.R.: telephone, (979) 845-3373; fax, (979) 845-9452; e-mail, raushel@tamu.edu. S.C.A.: telephone, (718) 430-2746; fax, (718) 430-8565; e-mail, almo@aecom.yu.edu.

[1]Abbreviations: URI, uronate isomerase; KDG, 2-keto-3-deoxy-D-gluconic acid; KDG-6-P, 2-keto-3-deoxy-6-phospho-D-gluconic acid; MDH, mannonate dehydrogenase; ICP-MS, inductively coupled plasma mass spectrometry; PDB, Protein Data Bank; rmsd, root-mean-square deviation.

© 2009 American Chemical Society
Published on Web 08/14/2009

Scheme 1

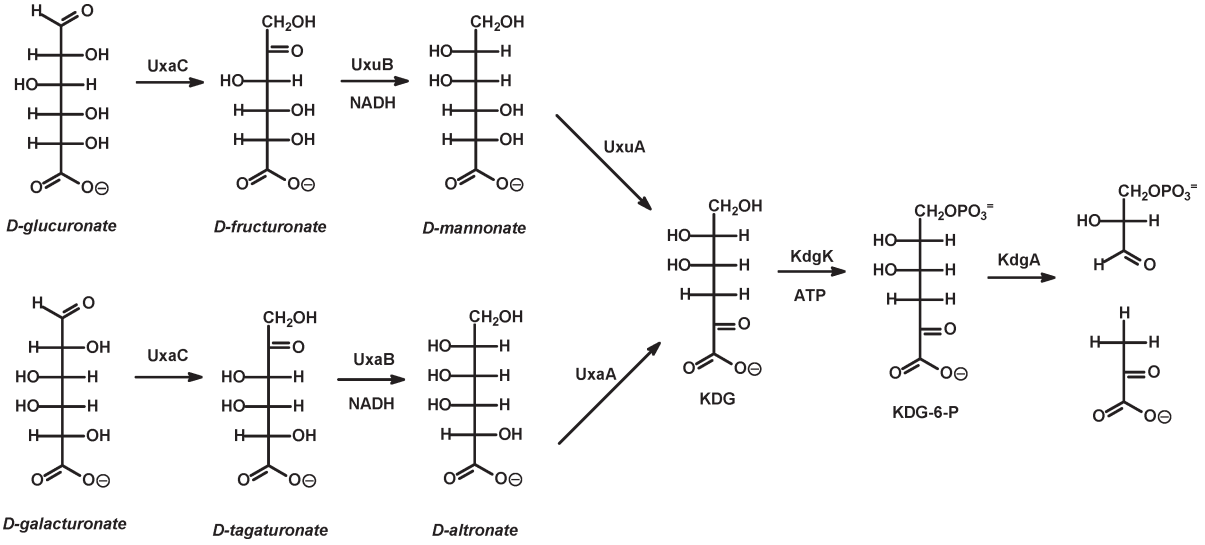

Scheme 2

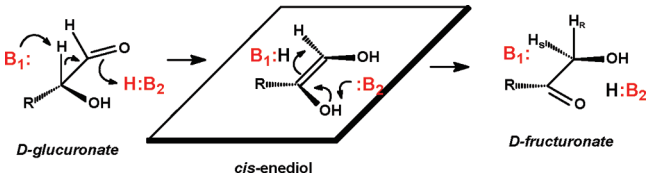

We have previously demonstrated that the hydrogen originally at C-2 of D-glucuronate is ultimately found at the *pro-R* position at C-1 of D-fructuronate and that this hydrogen slowly exchanges with solvent (*12*). These results are consistent with a proton transfer mechanism with a *cis*-enediol intermediate. The general mechanism, shown in Scheme 2, indicates a requirement for at least two residues that participate in the transformation of D-glucuronate into D-fructuronate. A general base ($:B_1$) abstracts the proton from C-2 of D-glucuronate, and a general acid ($H:B_2$) facilitates the transfer of a proton to the carbonyl oxygen at C-1 to produce the *cis*-enediol intermediate. In the subsequent step, the ketose product is generated by the transfer of a proton from the hydroxyl group at C-2 of the proposed intermediate and protonation of C-1 by $H:B_1$. For compounds such as D-glucuronate, the enzymatic transformation is made more complicated by the fact that in solution the substrate exists almost entirely as a mixture of two anomeric cyclic hemiacetals.

This paper focuses on a determination of the chemical mechanism for the isomerization reaction catalyzed by URI from *Escherichia coli*. The rate-limiting steps have been interrogated by measuring the primary kinetic isotope effects with [2-^{2}H]-D-glucuronate and solvent isotope effects with D_2O for the wild-type and mutant enzymes. The rate limitation imposed by product release has been examined using solvent viscosity effects. The identity of the residues involved in the proton transfer events has been probed by pH−rate profiles and characterization of the kinetic constants for mutant enzymes. These approaches have been augmented by the determination of the X-ray structure of a uronate isomerase from *Bacillus halodurans* (Bh0493) in the presence of D-glucuronate, D-fructuronate, and two mimics of the *cis*-enediol intermediate.

Scheme 3

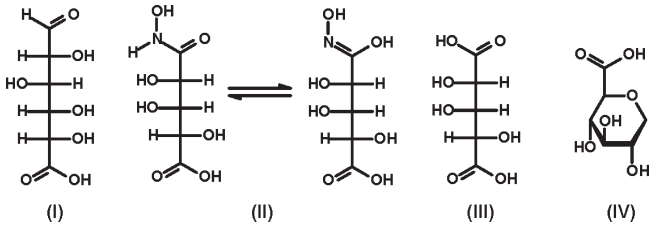

MATERIALS AND METHODS

Materials. D-Glucuronic acid (**I**), NADH, buffers, and all other chemicals were purchased from Sigma-Aldrich or Acros, unless otherwise stated. D-Arabinaric acid (**III**) and the monohydroxamate derivative of this compound (**II**) were synthesized as previously described (*12*). 2,6-Anhydro-L-gulonic acid (**IV**) was synthesized starting from L-xylose (*13*, *14*). The structures of these compounds are presented in Scheme 3. Oligonucleotide syntheses and DNA sequencing were performed by the Gene Technologies Lab of Texas A&M University. Metal analyses were conducted using inductively coupled plasma mass spectrometry (ICP-MS) as previously described (*12*).

Site-Directed Mutagenesis. Site-directed mutagenesis of URI was performed using the QuikChange mutagenesis kit from Stratagene. The following mutants were obtained by this method: H33N, H33A, H35N, H35A, H59N, H59A, Y60F, Y60A, R186K, R186M, D238N, H297N, R302K, R302M, H297A, W381F, W381A, D412N, D412A, R414K, and R414M. The mutations were confirmed by DNA sequencing of the modified plasmids.

Protein Expression and Purification. The *uxaC* gene encoding uronate isomerase in *E. coli* was cloned into the pET28 expression vector. The protein was expressed in *E. coli* strain BL21(DE3) and purified as previously described (*12*). The enzymes contained up to 1 equiv of zinc (depending on the mutant) as measured by ICP-MS.

Enzyme Assays. The conversion of D-glucuronate to D-fructuronate by URI was coupled to the reduction of D-fructuronate with NADH by mannonate dehydrogenase (MDH) as previously described (*12*). The assays were monitored spectrophotometrically by following the decrease in absorbance at 340 nm. The standard assay conditions included 50 mM HEPES (pH 8.0), varying

Table 1: Data Collection and Refinement Statistics for Crystals of the Complexes of Uronate Isomerase from *B. halodurans* with Various Ligands

	URI· D-arabinarate	URI· D-arabinarate	URI· arabinohydroxamate	URI· D-glucuronate	URI· D-fructuronate
Data Collection					
space group	*R*32	*C*2	*R*32	*C*2	$P4_122$
no. of molecules in the asymmetric unit	2	12	2	12	3
cell dimensions					
a, *b*, *c* (Å)	149.35, 149.35, 254.16	274.82, 156.52, 185.96	149.30, 149.30, 254.02	274.09, 156.88, 185.21	84.35, 99.14, 126.31
β (deg)		116.20		115.78	
resolution (Å)	2.2	2.2	2.2	2.1	1.9
no. of unique reflections	55294	352288	55174	404122	128635
R_{merge}	0.058	0.065	0.071	0.074	0.086
$I/\sigma I$	27.1	19.3	20.6	15.2	17.1
completeness (%)	99.7	98.8	99.8	98.7	93.9
Refinement					
resolution (Å)	25.0−2.2	25.0−2.2	25.0−2.2	25.0−2.1	25.0−1.9
R_{cryst}	0.218	0.213	0.204	0.227	0.213
R_{free}	0.238	0.245	0.226	0.258	0.241
no. of protein atoms	6766	40860	6744	40860	10164
no. of waters	259	1880	312	1824	572
rmsd for bond lengths (Å)	0.007	0.006	0.007	0.006	0.006
rmsd for bond angles (deg)	1.3	1.3	1.3	1.3	1.3
bound inhibitor	D-arabinarate	D-arabinarate	arabinohydroxamate	D-glucuronate	D-fructuronate
no. of inhibitor atoms	24	144	26	156	39
bound ions	$4Zn^{2+}$, $2CO_3^{2-}$, $2Cl^-$	$12Zn^{2+}$, $12CO_3^{2-}$, $4Na^+$, $4Cl^-$	$4Zn^{2+}$, $2CO_3^{2-}$, $2Cl^-$	$12Zn^{2+}$, $12CO_3^{2-}$, $4Cl^-$	$4Zn^{2+}$, $3CO_3^{2-}$, $1Cl^-$
PDB entry	3HK5	3HK7	3HK8	3HK9	3HKA

concentrations of D-glucuronate, 0.2 mM NADH, excess MDH, and URI in a final volume of 250 μL. The pH dependence of the kinetic parameters, k_{cat} and k_{cat}/K_m, was measured over the pH range of 5.3−10.3 at 0.20 pH intervals. The buffers used for the pH−rate profiles were MES, PIPES, HEPES, CHES, and CAPS. The pH values were recorded after the completion of the assays. The effects of solvent viscosity on the kinetic constants were determined at pH 8.0 using sucrose as the microviscogen at 25 °C. The concentrations of sucrose were 0, 10, 14, 20, 24, and 32% (w/w), and the corresponding relative viscosities were 1, 1.3, 1.5, 1.9, 2.2, and 3.2 (*15*, *16*). The solvent isotope effects on the kinetic parameters for URI and two mutant enzymes (D412N and R414M) were measured in 99% D_2O at pD 8.4. The primary deuterium kinetic isotope effects were obtained by direct comparison of the kinetic constants at pH 8.0 for [2-^{1}H]-D-glucuronate and [2-^{2}H]-D-glucuronate.

Preparation of [2-^{2}H]Glucuronic Acid. [2-^{2}H]-D-Glucuronate was prepared from [2-^{2}H]-D-glucose in three steps. The [2-^{2}H]-D-glucose was refluxed in methanol in the presence of dry Dowex-50(H^+) for 12 h to form a mixture of α- and β-methyl [2-^{2}H]-D-glucopyranoside (*17*). The solvent was removed under reduced pressure to yield crystals of the pure α-anomer. Methyl [2-^{2}H]-α-D-glucopyranoside was quantitatively oxidized at C-6 using a 2,2,6,6-tetramethyl-1-piperidinyloxy/sodium bromide/sodium hypochlorite mixture at pH 10, to form methyl [2-^{2}H]-α-D-glucuronopyranoside (*18*, *19*). The product was washed with methanol and purified using a column of DEAE-Sephadex with a gradient of sodium bicarbonate. The fractions containing the desired product were evaporated to dryness. The methyl [2-^{2}H]-D-glucuronopyranoside was demethylated with concentrated HCl at 4 °C and the pH adjusted to ~10 with sodium hydroxide. The concentration of [2-^{2}H]-D-glucuronate was determined enzymatically and was produced in an overall yield of 46%. The products from each step in the synthesis were characterized by ^{1}H and ^{13}C NMR and mass spectrometry.

Data Analysis. The kinetic parameters, k_{cat} and k_{cat}/K_m, for uronate isomerase with D-glucuronate as the substrate were determined by fitting the initial velocity data to eq 1

$$v/E_t = (k_{cat}[A])/(K_a + [A]) \quad (1)$$

where v is the initial velocity, E_t is the total enzyme concentration, k_{cat} is the turnover number, [A] is the substrate concentration, and K_m is the Michaelis constant. The profiles for the variation of k_{cat} or k_{cat}/K_m with pH were fit to eq 2

$$\log y = \log[c/(1 + H/K_a + K_b/H)] \quad (2)$$

where c is the pH-independent value of y, K_a and K_b are the dissociation constants of the ionizable groups, and H is the proton concentration. The competitive inhibition patterns were fit to eq 3

$$v/E_t = (k_{cat}[A])/[K_a(1 + I/K_{is}) + [A]] \quad (3)$$

where K_{is} is the slope inhibition constant and I is the concentration of the inhibitor.

Crystallization and Data Collection. Five different crystalline complexes (Table 1) were grown by the hanging drop method at room temperature for Bh0493 from *B. halodurans*: (a) complex with D-arabinarate, crystal form 1; (b) complex with D-arabinarate, crystal form 2; (c) complex with arabinohydroxamate; (d) complex with D-glucuronate; and (e) complex with D-fructuronate. The initial protein solution for all five crystallizations contained Bh0493 (16 mg/mL) in 10 mM HEPES (pH 7.5), 150 mM NaCl, 10 mM methionine, 10% glycerol, 1.0 mM DTT,

0.2 mM $ZnCl_2$, and the corresponding substrate or inhibitor at 40 mM. The crystallization conditions were as follows. For the Bh0493·D-arabinarate complex (form 1), the protein solution contained 40 mM D-arabinarate and the precipitant contained 25% PEG 3350, 0.1 M Tris (pH 8.5), and 0.2 M NaCl. Crystals appeared in 4−5 days and exhibited diffraction consistent with space group *R*32, with two copies of the complex per asymmetric unit. For the Bh0493·D-arabinarate complex (form 2), the protein solution contained 40 mM D-arabinarate and the precipitant contained 20% PEG 3350 and 0.2 M sodium citrate (pH 6.0). Crystals appeared in 4 days and exhibited a diffraction pattern consistent with space group *C*2, with 12 copies of the complex per asymmetric unit. For the Bh0493·arabinohydroxamate complex, the protein solution contained 40 mM arabinohydroxamate and the precipitant contained 25% PEG 3350, 0.1 M Tris (pH 8.5), and 0.2 M NaCl. Crystals appeared in 2 days and exhibited a diffraction pattern consistent with space group *R*32, with two copies of the complex per asymmetric unit. For the Bh0493·D-glucuronate complex, the protein solution contained 40 mM D-glucuronate and the precipitant contained 20% PEG 3350 and 0.2 M ammonium citrate (pH 6.0). For this complex, the protein solution was incubated on ice with D-glucuronate for 2 h before crystallization. The crystals appeared in 9 days and exhibited diffraction consistent with space group *C*2, with 12 copies of the complex per asymmetric unit. For the Bh0493·D-fructuronate complex, the protein solution was incubated on ice for ~2 months with 40 mM D-glucuronate before crystallization. The precipitant contained 25% PEG 3350, 0.1 M Tris (pH 8.5), and 0.2 M NaCl. Crystals appeared in 2 weeks and exhibited diffraction consistent with space group $P4_122$, with three copies of the complex per asymmetric unit.

Prior to data collection, the crystals of all Bh0493 complexes (Table 1) were transferred to cryoprotectant solutions composed of their mother liquids and 20% glycerol and flash-cooled in a nitrogen stream. All data sets were collected at the NSLS X4A beamline (Brookhaven National Laboratory) on an ADSC CCD detector (Table 1). Diffraction intensities were integrated and scaled with DENZO and SCALEPACK (*20*). The data collection statistics are given in Table 1.

Structure Determination and Model Refinement. All five URI structures (Table 1) were determined by molecular replacement with the fully automated molecular replacement pipeline BALBES (*21*), using only input diffraction and sequence data. The native uronate isomerase from *B. halodurans* (PDB entry 2Q08) was used by BALBES as a template in all five structure determinations. Partially refined structures of all URI crystal forms (Table 1) were output from BALBES without manual intervention. Several iterative cycles of refinement were performed for each crystal form, including manual model rebuilding with TOM (*22*), refinement with CNS (*23*), automatic model rebuilding with ARP (*24*), and solvent building with the CCP4 suite (*25*).

The rhombohedral crystal form of the Bh0493·D-arabinarate complex contains two copies of the complex in the asymmetric unit of the cell; the monoclinic crystal form of the same complex contains 12 copies of the complex in the asymmetric unit packed as four trimers. The first residue and last 13 residues of every molecule are disordered in the first crystal form of this complex. The four N-terminal residues and last 14 residues are disordered in every molecule of the second crystal form of the Bh0493·D-arabinarate complex. The disordered residues are not included in the final models. The asymmetric unit of the

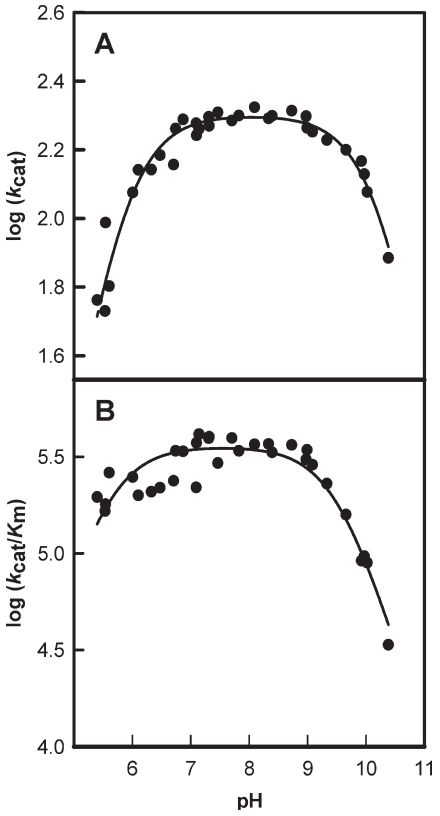

FIGURE 1: pH−rate profile for the wild-type uronate isomerase from *E. coli* containing 1 equiv of zinc. The data were fit to eq 2: (A) plot of log k_{cat} vs pH and (B) plot of log k_{cat}/K_m vs pH.

Bh0493·arabinohydroxamate crystalline complex contains two molecules of the complex, where the first residue and the last 14 residues of every molecule are disordered. The asymmetric unit of the Bh0493·D-glucuronate crystalline complex contains 12 copies of the complex packed as four trimers. The first residue and the last 13 residues are disordered in every molecule of this complex. The asymmetric unit of the Bh0493·D-fructuronate crystalline complex contains one trimer of the complex. The first two residues and last 14 residues are disordered in every molecule and are not included in the final models. This complex was produced by a long incubation and subsequent cocrystallization of Bh0493 with D-glucuronate, but the electron density of the bound inhibitor can be interpreted only as the product, D-fructuronate. The Zn^{2+} ions bound in the active sites were clearly visible in every molecule of every URI complex listed in Table 1. Additional ions (Na^+, Zn^{2+}, and Cl^-) located on the local 3-fold axis of every Bh0493 trimer also exhibited good density in all five URI crystalline complexes. Final crystallographic refinement statistics for all of the URI complexes are provided in Table 1.

RESULTS

Requirement for a Divalent Cation. The importance of a metal ion for the catalytic activity of uronate isomerase was reinvestigated. The apoenzyme was prepared and subsequently tested for enzymatic activity using D-glucuronate as the substrate. The wild-type URI from *E. coli* was found to contain 0.9 equiv of zinc after purification. This protein (3 mL) at a concentration of 3.0 mg/mL was dialyzed against 1 L of dialysis buffer containing 20 mM dipicolinate in 50 mM MES (pH 6.0). The buffer was changed three times over the course of 48 h, and then the catalytic activity and metal content of the enzyme were determined. The

Table 2: Kinetic Parameters and Metal Content of Mutants of URI from *E. coli*[a]

enzyme	k_{cat} (s^{-1})	K_m (mM)	k_{cat}/K_m (M^{-1} s^{-1})	URI/Zn
wild type	196 ± 6	0.50 ± 0.05	$(4.0 \pm 0.4) \times 10^5$	0.90
H33N (H26)[b]	2.1 ± 0.1	$(5.0 \pm 0.4) \times 10^{-2}$	$(4.7 \pm 0.4) \times 10^4$	0.07
H33A	0.60 ± 0.01	0.20 ± 0.01	$(3.0 \pm 0.2) \times 10^3$	0.20
H35N (H28)	4.0 ± 0.2	9.4 ± 1.1	$(4.3 \pm 0.5) \times 10^2$	< 0.05
H35A	0.70 ± 0.04	39 ± 5	18 ± 2	< 0.05
H59N (H49)	15 ± 1	0.70 ± 0.04	$(2.1 \pm 0.1) \times 10^4$	0.96
H59A	0.60 ± 0.01	0.70 ± 0.07	$(8.3 \pm 0.1 \times 10^2$	0.95
Y60F (Y50)	21.7 ± 0.1	0.16 ± 0.01	$(1.4 \pm 0.1) \times 10^5$	0.8
Y60A	13.9 ± 0.1	0.21 ± 0.01	$(6.6 \pm 0.3) \times 10^4$	0.8
R186K (R170)	54 ± 2	2.6 ± 0.2	$(2.1 \pm 0.2) \times 10^4$	0.94
R186M	4.7 ± 0.1	38 ± 3	$(1.3 \pm 0.1) \times 10^2$	0.91
D238N	60 ± 1	1.3 ± 0.1	$(4.6 \pm 0.1) \times 10^4$	0.70
H297N (M258)	30 ± 2	56 ± 5	$(5.0 \pm 0.5) \times 10^2$	1.00
H297A	10 ± 1	$(2.2 \pm 0.3) \times 10^2$	43 ± 7	0.41
R302K (K303)	160 ± 4	2.5 ± 0.2	$(6.3 \pm 0.5) \times 10^4$	0.90
R302M	180 ± 9	$(2.0 \pm 0.3) \times 10^2$	$(8.8 \pm 1.3) \times 10^2$	0.99
W381F (W325)	16 ± 1	1.7 ± 0.1	$(9.5 \pm 0.4) \times 10^3$	0.90
W381A	250 ± 6	21 ± 2	$(1.2 \pm 0.1) \times 10^4$	0.69
D412N (D355)	0.60 ± 0.01	1.00 ± 0.04	$(6.0 \pm 0.3) \times 10^2$	0.36
D412A	$(9.0 \pm 0.3) \times 10^{-3}$	0.40 ± 0.05	21 ± 3	0.12
R414K (R357)	5.8 ± 0.1	0.82 ± 0.02	$(7.1 \pm 0.2) \times 10^3$	0.92
R414M	0.70 ± 0.01	1.4 ± 0.1	$(5.4 \pm 0.2) \times 10^2$	0.91

[a]These data were obtained at 30 °C and pH 8.0, with D-glucuronate as the substrate. [b]The corresponding residue numbers for Bh0493.

chelator effectively removed more than 98% of the bound zinc as indicated by ICP-MS. The activity of the enzyme was assayed with mannonate dehydrogenase and NADH to detect the formation of D-fructuronate in the presence of 10 μM dipicolinate. The apoenzyme exhibited less than 1% of the activity of the native enzyme with bound zinc. This result is at variance with our previous report which had concluded that the activity of uronate isomerase is independent of the presence or absence of divalent cations within the active site (*12*). The reason for this difference in results has not been determined but was perhaps due to contaminating divalent cations in the assay solution.

Inhibition by 2,6-Anhydro-L-gulonic Acid (***IV***). Compound **IV** was synthesized as a cyclic analogue mimic of the pyranose form of D-glucuronate. The inhibitory properties of **IV** were determined with the wild-type uronate isomerase from *E. coli* and *B. halodurans* (Bh0493). This compound was found to be a competitive inhibitor for both enzymes. The data were fit to eq 3, and the values of K_{is} were determined to be 45 ± 4 and 24 ± 2 μM for the URI from *E. coli* and Bh0493, respectively.

pH−Rate Profiles. The kinetic constants for the conversion of D-glucuronate to D-fructuronate were obtained as a function of pH. The pH−rate profiles for the effects of pH on k_{cat} and k_{cat}/K_m are presented in panels A and B of Figure 1, respectively. The pH profiles are bell-shaped and are consistent with a single functional group that must be unprotonated for activity and another functional group that must be protonated for catalytic activity. From a fit of the data to eq 2, the kinetic pK_a values from the k_{cat}/K_m plot are 5.5 ± 0.1 and 9.5 ± 0.1, respectively. From the plot of k_{cat} versus pH, kinetic pK_a values of 5.8 ± 0.1 and 10.2 ± 0.1 were obtained.

Site-Directed Mutants. Site-directed mutagenesis was utilized to identify the involvement of specific amino acids in metal binding, substrate recognition, and the catalytic mechanism of uronate isomerase. Conserved residues were chosen on the basis of the location within the active site of Bh0493, a uronate isomerase found in *B. halodurans*. His-33 and His-35 were mutated to investigate the importance of metal binding and the potential role of the divalent cation in catalytic activity. Mutations at either of these two resides resulted in the dramatic loss of affinity for the divalent cation and a significant reduction in catalytic activity. The diminution of catalytic activity for the mutants is more severe when these histidine residues are changed to alanine than to asparagine. The highly conserved histidine at the end of β-strand 5 (His-297) and the invariant aspartate at the end of β-strand 8 (Asp-412) were mutated to asparagine and alanine. For the mutations at His-297, there were substantial increases in the Michaelis constant. In contrast, with the mutation of Asp-412, the reduction in catalytic activity was more pronounced on k_{cat}. These four residues are broadly conserved in all members of the amidohydrolase superfamily.

Additional residues that are conserved among all of the known uronate isomerases were mutated as a probe of functional participation in binding and catalysis. These residues include Trp-381 from the conserved WWF motif after β-strand 7, His-59 and Tyr-60 after β-strand 1, and three conserved arginines (Arg-186, Arg-302, and Arg-414). Mutation of residues Trp-381 and Arg-302 resulted in increases in the value of K_m and small changes in k_{cat}, indicating that these residues most likely take part in substrate recognition and binding. For the methionine mutation at Arg-186, there were significant changes in both k_{cat} and k_{cat}/K_m. For His-59 and Arg-414, there were relatively small changes in K_m but drastic reductions in the value of k_{cat}. The kinetic constants for the mutants constructed for this investigation are listed in Table 2.

Kinetic Isotope Effects. Primary deuterium kinetic isotope effects on the isomerization of D-glucuronate were measured as a probe of the rate-limiting steps in the overall reaction mechanism. For the solvent deuterium isotope effects, the kinetic parameters were obtained for the wild-type enzyme in H_2O and D_2O with D-glucuronate as the substrate. The double-reciprocal plots are presented in Figure 2. The solvent isotope effects for $^{D_2O}k_{cat}$ and $^{D_2O}(k_{cat}/K_m)$ are 1.22 ± 0.02 and 1.10 ± 0.09, respectively. Solvent isotope effects were also determined for four of the site-directed mutants, H59N, Y60F, D412N, and R414M. The

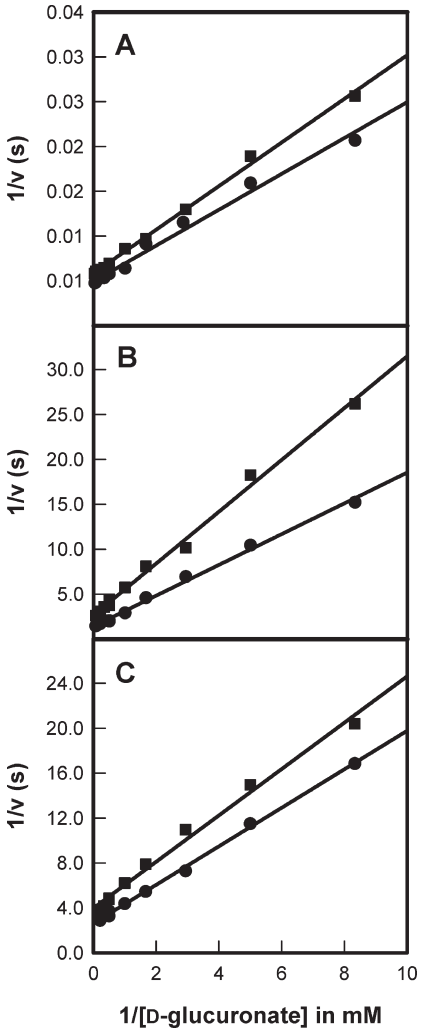

FIGURE 2: Double-reciprocal plots for the solvent isotope effect (H_2O vs D_2O), where $1/v$ (s) is plotted vs 1/[D-glucuronate] (mM^{-1}). The data sets in H_2O are represented by circles, and the squares correspond to the values obtained in D_2O: (A) wild-type enzyme, (B) R414M mutant, and (C) D412N mutant.

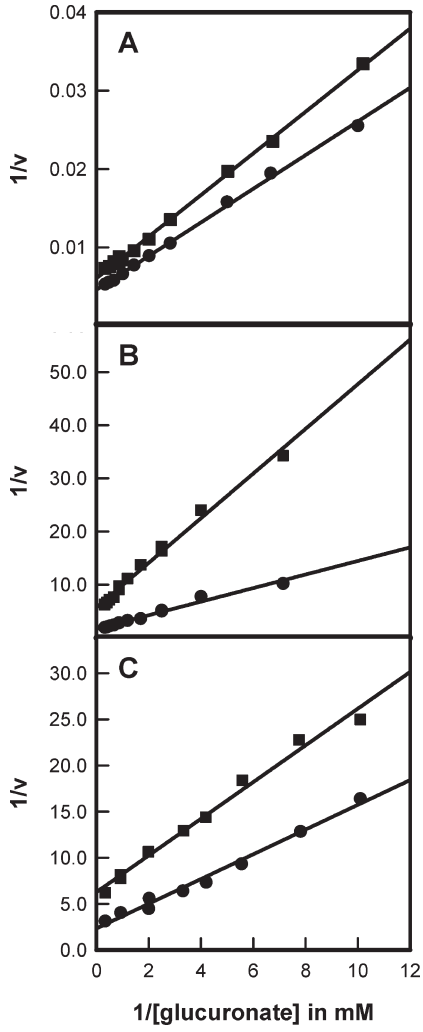

FIGURE 3: Primary isotope effects using protonated and deuterated D-glucuronate at the C-2 position are presented as double-reciprocal plots: (A) wild-type enzyme, (B) R414M mutant, and (C) D412N mutant. The data for the protonated substrate are represented as circles, and the values for the deuterated substrate are depicted as squares.

solvent isotope effects for the H59N mutant were 1.7 ± 0.1 for $^{D_2O}k_{cat}$ and 1.4 ± 0.1 for $^{D_2O}(k_{cat}/K_m)$, while the effects for the Y60F mutant were 2.1 ± 0.1 and 1.2 ± 0.1 for $^{D_2O}k_{cat}$ and $^{D_2O}(k_{cat}/K_m)$, respectively. For the D412N mutant, the solvent isotope effects were determined to be 1.3 ± 0.1 and 1.5 ± 0.2 for $^{D_2O}k_{cat}$ and $^{D_2O}(k_{cat}/K_m)$, respectively. For the R414M mutant, the solvent isotope effects were 1.8 ± 0.1 for $^{D_2O}k_{cat}$ and 2.0 ± 0.3 for $^{D_2O}(k_{cat}/K_m)$.

The primary deuterium isotope effects for abstraction of the proton from C-2 of D-glucuronate were determined for the wild-type enzyme and two mutants, D412N and R414M. The double-reciprocal plots are shown in Figure 3. For the wild-type enzyme, the primary deuterium isotope effects on k_{cat} and k_{cat}/K_m were determined to be 1.4 ± 0.1 and 1.2 ± 0.1, respectively. For the D412N mutant, the primary deuterium isotope effects were determined to be 2.0 ± 0.2 for $^{D}k_{cat}$ and 1.9 ± 0.3 for $^{D}(k_{cat}/K_m)$. For the R414M mutant, the isotope effect on k_{cat} was 3.2 ± 0.1 and the effect on k_{cat}/K_m was 3.5 ± 0.4.

Solvent Viscosity Effects. Alterations in solvent viscosity were utilized to probe the degree of rate limitation by the binding and dissociation of products and substrates on the kinetic constants of uronate isomerase (*15*). The effects of changes in solvent viscosity on k_{cat} and k_{cat}/K_m were made by the addition of sucrose (*26*). A plot of $^{o}k_{cat}/^{\eta}k_{cat}$ versus the relative solvent viscosity for the wild-type enzyme exhibits a slope of 0.72 ± 0.08. The slope for the effect of solvent viscosity on k_{cat}/K_m is 0.64 ± 0.05 for the wild-type enzyme. For the two mutant enzymes, D412N and R414M, the slopes for the effect of solvent viscosity on k_{cat} were found to be 0.07 ± 0.05 and 0.05 ± 0.01, respectively. For the effect on k_{cat}/K_m, the slopes were 0.03 ± 0.05 and −0.17 ± 0.02 with the D412N and R414M mutant enzymes, respectively. The kinetic data are presented in panels A and B of Figure 4.

Structures of Inhibitor Complexes. The crystal structure of Bh0493 from *B. halodurans* was previously determined in the absence of bound substrates or inhibitors [PDB entry 2Q08 (*3*)]. In that structure, zinc is bound in the active site and coordinated to two histidines from β-strand 1 (H26 and H28) and the invariant aspartate found at the end of β-strand 8 (D355). The structure of Bh0493 was determined in the presence of the substrates D-glucuronate (**I**), D-fructuronate, and two inhibitors that mimic the proposed *cis*-enediol(ate) intermediate, D-arabinarate (**III**) and its hydroxamate derivative (**II**). Portions of the electron density maps that show the D-glucuronate and D-fructuronate in the active site of Bh0493 are presented in panels A and B of Figure 5, respectively. These compounds

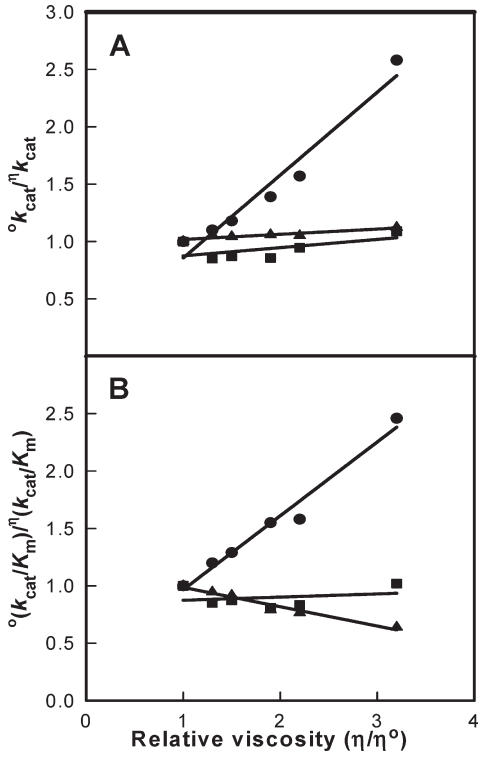

FIGURE 4: Effect of viscosity on the relative values of k_{cat} (A) and k_{cat}/K_m (B) using sucrose as the microviscogen. The circles indicate data for the wild-type enzyme from *E. coli*; the squares represent the data set for the D412N mutant, and the triangles denote the values for the R414M mutant.

occupy the active site in a similar manner and interact with the same set of amino acid residues. Stereoscopic images of the active site complexes for compounds **I**, **II**, and **III** are presented in panels A−C of Figure 6, respectively, and the distances between specific amino acid residues and the bound ligands are provided in panels A−C of Figure 7, respectively.

In the complex with D-glucuronate, the substrate is bound in the open chain configuration. The terminal carboxylate is ion-paired with the guanidino group of Arg-170, and there is a monodentate coordination with the bound zinc. The zinc is also ligated with the hydroxyl group attached to C-5 of the substrate. The hydroxyl group at C-4 does not make any specific interactions with the protein, which is consistent with the observation that both D-glucuronate and D-galacturonate are substrates for this enzyme (*1*). The hydroxyl at C-3 interacts with both Arg-357 and His-49. The nearest residue to the hydroxyl at C-2 of D-glucuronate is Arg-357. The hydroxyl group from Tyr-50 hydrogen bonds with the carbonyl group at C-1 of the substrate. The closest residue to the hydrogen that is abstracted from C-2 of D-glucuronate is the side chain carboxylate of Asp-355. Similar interactions are found in the complexes with D-fructuronate, D-arabinarate, and the corresponding hydroxamate derivative. The D-fructuronate complex was identified in a crystal that was grown after a long incubation and subsequent cocrystallization of Bh0493 with D-glucuronate.

DISCUSSION

The uronate isomerase from *E. coli* has previously been shown to catalyze the isomerization of D-glucuronate and D-galacturonate to D-fructuronate and D-tagaturonate, respectively (*1*, *2*). With D-glucuronate, the hydrogen at C-2 was shown to be

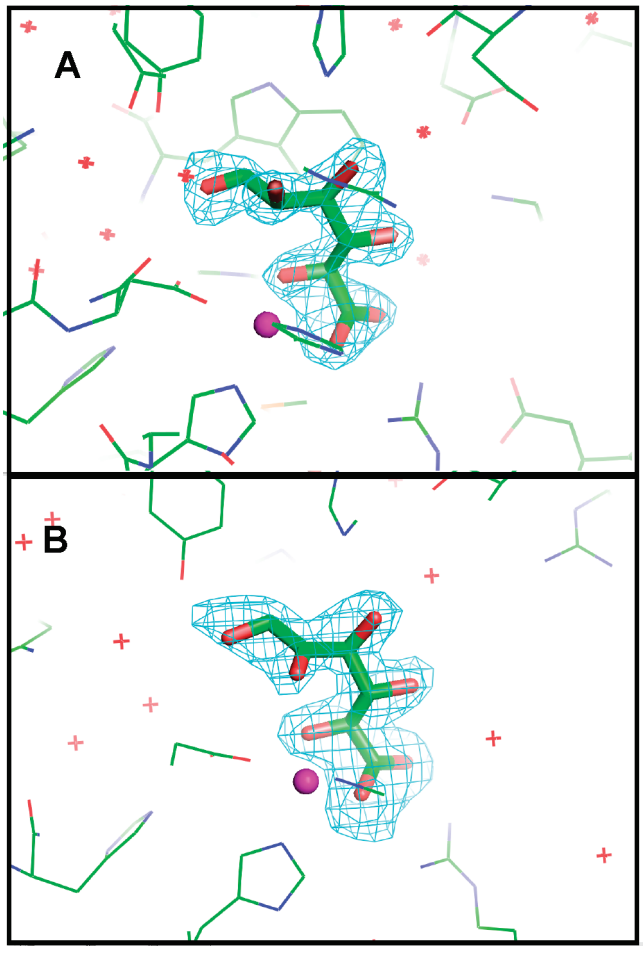

FIGURE 5: View of the active site structures of Bh0493 with bound ligands: (A) D-glucuronate and (B) D-fructuronate. Omit electron density maps ($F_o - F_c$) are contoured at 3.5σ. The corresponding ligands were omitted from the model, and the remainder of the unit cell was subjected to a cycle of simulated annealing with CNS at 3000 °C.

transferred to the *pro-R* position at C-1 of the product (*12*). This hydrogen exchanges with solvent at a rate that is 4 orders of magnitude slower than the rate of net interconversion of substrate and product. These results were interpreted to be consistent with a reaction mechanism that was initiated by proton abstraction at C-2, formation of a *cis*-enediol(ate) intermediate, and subsequent reprotonation at C-1 (*12*). This minimal reaction mechanism thus requires at least two different residues within the active for these proton transfers. A general base (B_1:) is required for the removal of the proton at C-2 and delivery to C-1, and a general acid (B_2:H) is needed to shuttle a proton between the oxygens attached to C-1 and C-2 of the substrate/product pair. This transformation has been summarized in Scheme 2. A requirement for a minimum of two amino acids that must be in a specific state of protonation is experimentally supported by the measurement of the effects of pH on the magnitude of k_{cat} and k_{cat}/K_m for the conversion of D-glucuronate to D-fructuronate. The pH−rate profiles for both k_{cat} and k_{cat}/K_m are bell-shaped and indicate that one residue must be unprotonated and another protonated for catalytic activity. In these profiles, the general base has a kinetic pK_a between 5.5 and 5.8, whereas the general acid has a kinetic pK_a between 9.5 and 10.2. Candidates for these residues were identified through the elucidation of the three-dimensional crystal structure of a uronate isomerase from

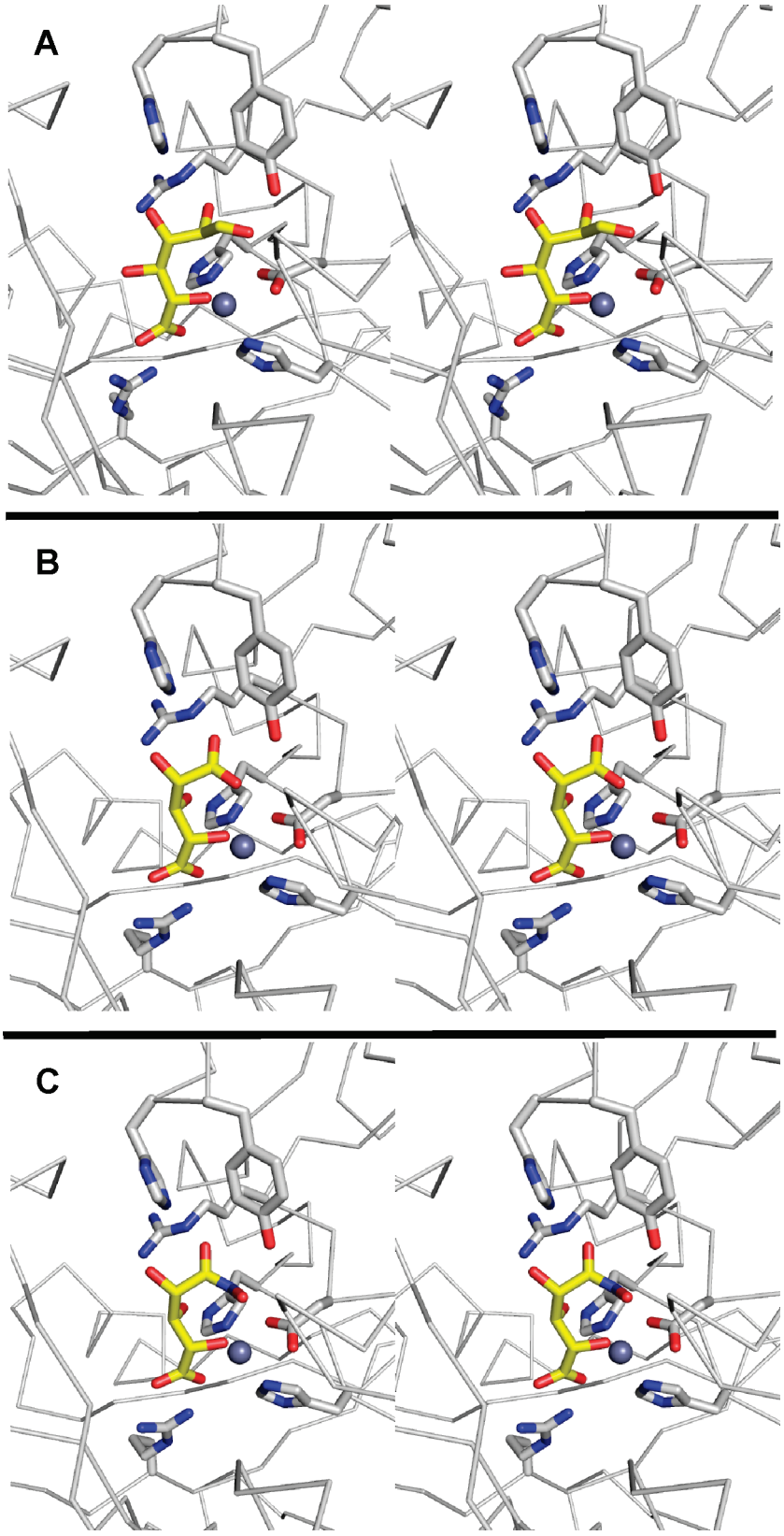

FIGURE 6: Stereoview images of Bh0493 in the presence of bound (A) D-glucuronate (**I**), (B) arabinarate (**III**), and (C) hydroxamate of arabinarate (**II**). This figure was created with PyMOL version 0.99.

B. halodurans (Bh0493) in the presence of D-glucuronate, D-fructuronate, and two mimics of the *cis*-enediol(ate) intermediate.

The crystal structure of Bh0493 determined with D-glucuronate has identified those residues in the active site that interact directly with the substrate. In this structure, the zinc is ligated by three amino acids from the protein: the two conserved histidine residues from β-strand 1 and the aspartate from β-strand 8. The C-6 carboxylate group of the substrate is ligated to the zinc and also ion-paired with Arg-170. The hydroxyl group from C-5 is ligated to the zinc in the active site and hydrogen bonded to the

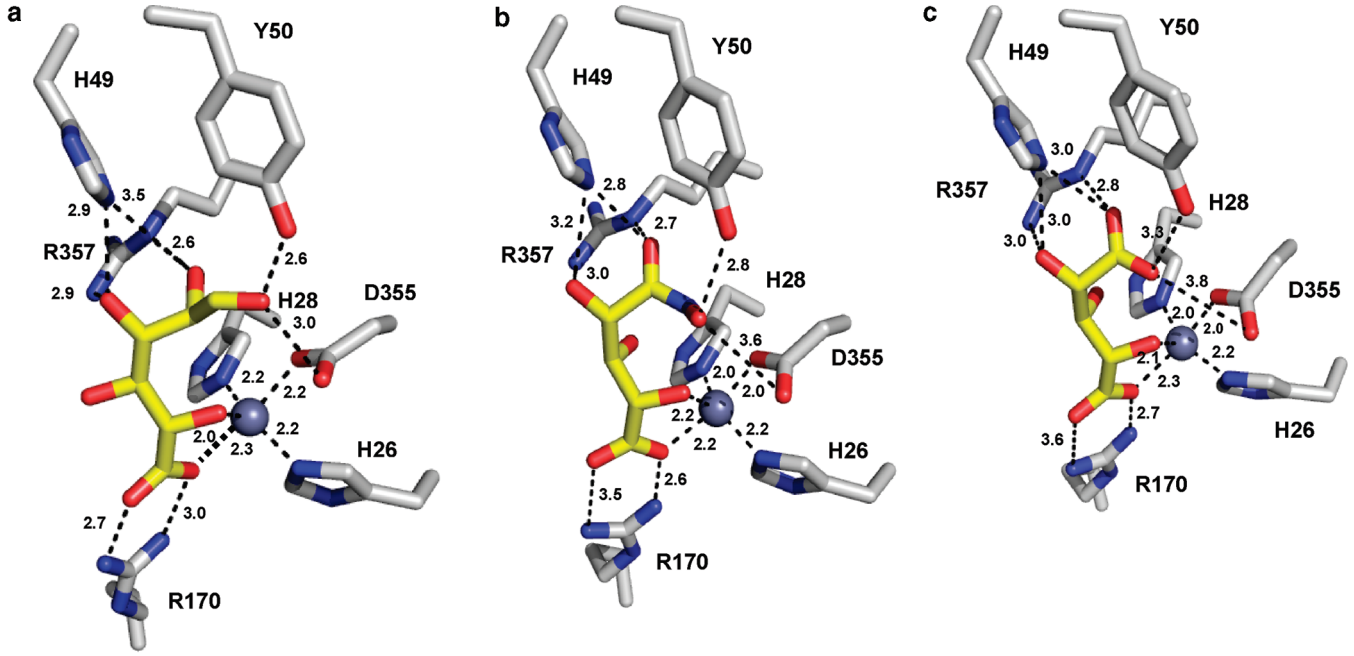

FIGURE 7: Active site of Bh0493 with (A) D-glucuronate, (B) hydroxamate of D-arabinarate, and (C) D-arabinarate. Interactions between the enzyme and ligand are shown with the distances.

aspartate from β-strand 8. At the other end of the substrate, Arg-357 hydrogen bonds with the two hydroxyls from C-3 and C-2. The phenolic group of Tyr-50 forms a hydrogen bond with the carbonyl group at C-1. The closest residue from the protein to the hydrogen at C-2 that must be abstracted during the chemical transformation is Asp-355 at 3.15 Å. In addition, His-49 is within hydrogen bonding distance of the hydroxyl at C-2 in the hydroxamate inhibitor (**II**) but not in the complex with the bound D-glucuronate (**I**). Thus, the most likely residues that are required for the isomerization reaction (in Bh0493) are His-49, Tyr-50, Asp-355, and Arg-357. In the *E. coli* enzyme, these residues are equivalent to His-59, Tyr-60, Asp-412, and Arg-414, respectively. These residues, in addition to His-33 and His-35 (ligands to the zinc), Arg-186 (equivalent to R170 in Bh0493), His-297 (a conserved histidine at the end of β-stand 5 in most members of the amidohydrolase superfamily), Arg-302, and Trp-381, were mutated as probes of functional significance.

The mutation of specific residues within the active site of URI results in significant perturbations to the magnitude of the kinetic constants for substrate turnover. Changes to either of the two histidine residues that originate from the end of β-strand 1 weaken the binding of zinc to the active site, and this results in a diminution of catalytic activity. This observation is consistent with the proposed role of zinc in the direct ligation of the substrate through the C-6 carboxylate and the hydroxyl from C-5. A drastic reduction in the affinity of the substrate occurs with the mutation of Arg-186 to methionine. In this case, the K_m for the substrate increases by nearly 2 orders of magnitude and the value of k_{cat}/K_m is reduced by more than 3 orders of magnitude. This result is consistent with an ion pair interaction between the C-6 carboxylate and the guanidino group of Arg-186 (R170 in Bh0493) that is observed in the X-ray structure of Bh0493. There is also a substantial increase in the K_m for D-glucuronate when His-297 is mutated to alanine or asparagine. This residue originates from the end of β-strand 5 and is highly conserved in nearly all members of the amidohydrolase superfamily, but this residue is not conserved in Bh0493; thus, it is not easy to discern the effect on the structure of URI from *E. coli*.

Scheme 4

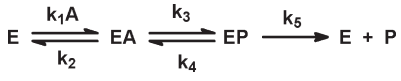

The most dramatic reductions in k_{cat} occur with the mutation of Asp-412 to alanine or Arg-414 to methionine. Arg-414 is equivalent to Arg-357 from Bh0493, which is hydrogen bonded to the C-2 and C-3 hydroxyls of the bound D-glucuronate. Therefore, this residue is a suitable candidate for assisting in the movement of the proton from the hydroxyl at C-2 during the transformation to D-fructuronate. The other candidate for this process is the phenolic side chain from Tyr-60. This group is hydrogen bonded to the carbonyl oxygen at C-1 of D-glucuronate in the X-ray crystal structure. Mutation of Tyr-60 to phenylalanine results in reductions in k_{cat} and k_{cat}/K_m of ~1 order of magnitude. The only residue from the protein that is suitably positioned to function as the general base for the abstraction of the proton from C-2 and delivery to C-1 is Asp-412. Many members of the amidohydrolase superfamily that catalyze hydrolytic reactions have been shown to use this residue from the end of β-strand 8 to abstract a proton from the hydrolytic hydroxide or water (*6*, *8*, *27*, *28*).

Changes in solvent viscosity and isotopic substitution were used to address the degree of rate limitation on the bond breaking steps and product release (*15*, *16*). A simplified kinetic mechanism for the conversion of substrate to product for the uronate isomerization reaction is presented in Scheme 4, where EA represents the enzyme−glucuronate complex and EP represents the enzyme−fructuronate complex. In this mechanism, the expression for k_{cat} is given by $(k_3k_5)/(k_3 + k_4 + k_5)$. If one assumes that k_5 is inversely proportional to the relative solvent viscosity, then the value of k_5, relative to the sum of k_3 and k_4, can be determined from a plot of the ratio of ${}^{o}k_{cat}/{}^{\eta}k_{cat}$ as a function of the relative solvent viscosity, η. The slope of this plot is equal to

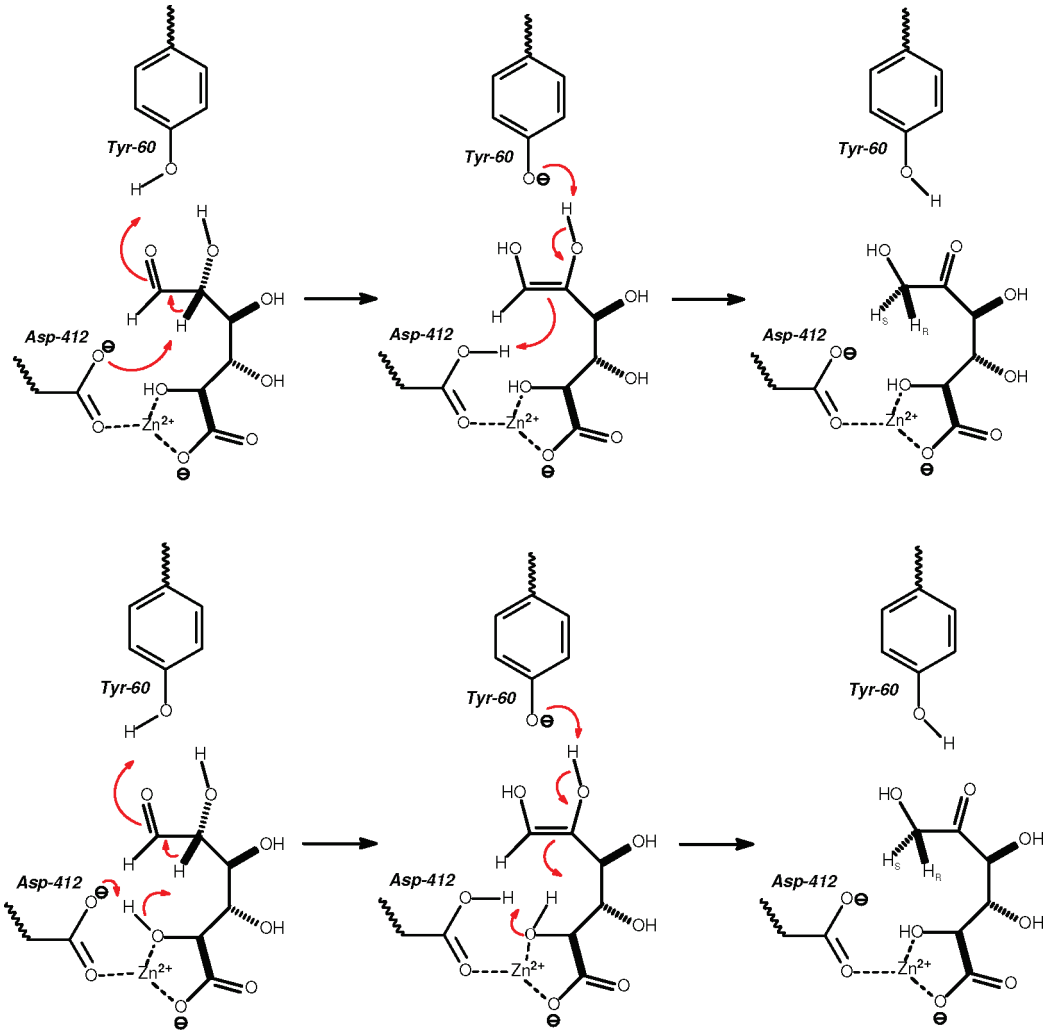

FIGURE 8: Proposed mechanisms for the isomerization of D-glucuronate by URI.

$(k_3 + k_4)/(k_3 + k_4 + k_5)$. For the wild-type enzyme, the slope was found to be ~0.7, and thus, the sum of k_3 and k_4 is greater than the rate of the product release step, k_5. This result is consistent with the release of the product as the rate-limiting step for the wild-type enzyme and the relatively small primary isotope effect for [2-^{2}H]-D-glucuronate. With the D412N and R412M mutants, the slope of this plot, for changes in the relative value of k_{cat} as a function of solvent viscosity, is reduced substantially. This result is consistent with a significant reduction in the rate constants for the interconversion of the substrate/product pair to the point where k_5 is now greater than the sum of k_3 and k_4. This result is also consistent with the significant increase in the value of $^D k_{cat}$. With the D412N and R414M mutants, the primary isotope effects are 2.0 and 3.2, respectively, and thus, with these two mutants, the interconversion of the substrate/product pair is substantially rate-limiting.

Mechanism of Action. On the basis of the X-ray crystal structure of Bh0493 in the presence of the bound substrate, the catalytic properties of selected site-directed mutants and the stereochemical constraints for the conversion of D-glucuronate to D-fructuronate, a minimal chemical mechanism can be written for uronate isomerase. In the proposed mechanism for URI from *E. coli*, D-glucuronate is bound in the active site through electrostatic interactions to five highly conserved amino acid residues and the divalent cation. The carboxylate group at C-6 is coordinated to the divalent cation and Arg-186. The hydroxyl group at C-5 is also coordinated to the zinc. The hydroxyl groups at C-3 and C-2 interact with the side chain guanidino group of Arg-414, and the hydroxyl at C-2 is also apparently able to form a hydrogen bond to His-59. The carbonyl group at C-1 is hydrogen bonded to the phenolic oxygen of Tyr-60. The pH−rate profiles for URI are consistent with two amino acid residues that must be in a specific state of protonation for catalytic activity. The general base, with a kinetic pK_a of approximately 5.8, is consistent with Asp-412. This residue is conserved in all members of the amidohydrolase superfamily, and for those enzymes that catalyze hydrolytic reactions, it has been shown to initiate proton transfers from water/hydroxide to the leaving group (*6*, *8*, *27*, *28*). The general acid, with a kinetic pK_a of approximately 10.2 from the pH−rate profiles, may be due to Tyr-60, but it is difficult to exclude a role for Arg-414.

In the simplest mechanism, D-glucuronate binds in the open chain conformation in the active site and then Asp-412 abstracts the proton from C-2 as the carbonyl group of C-1 is protonated by Tyr-60 to form a *cis*-enediol intermediate. In the subsequent step, Tyr-60 abstracts the proton from the hydroxyl at C-2 as Asp-414 delivers a proton to C-1 with *pro-R* stereochemistry. It should be noted that the mutation of Tyr-60 to alanine or phenylalanine diminishes k_{cat} by a factor of only 10. This reduction in rate is perhaps smaller than what may be expected for this role in catalysis. However, the lack of a primary deuterium isotope effect for the wild-type enzyme indicates that

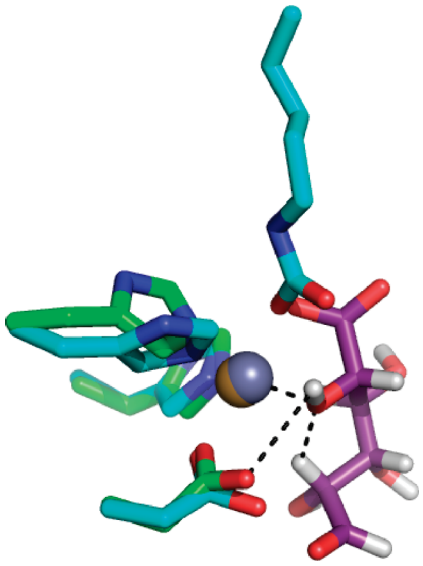

FIGURE 9: Structural alignment for portions of the active sites of Bh0493 (green) and DHO from *E. coli* (blue). The α-metal (M_α) is shown as a yellow sphere for Bh0493 and as a gray sphere for DHO. The bound D-glucuronate for Bh0493 is colored purple. The interactions between the C-5 oxygen of D-glucuronate and M_α, the C-2 hydrogen, and Asp-412 are represented by dashed lines. The other ligands to the metal ion are shown as stick representations, including the HxH motif from β-strand 1 and aspartate from β-strand 8. The C-6 oxygen of D-glucuronate aligns closely with the position occupied by one of the oxygens from the carboxyl group of the carboxylated lysine from strand 4 of DHO. The C-5 hydroxyl of D-glucuronate is oriented in the same position as the bridging hydroxide in the DHO structure.

the chemical step is not rate-limiting. In addition, a water molecule may substitute for the phenolic group in the mutant enzymes. Additional mechanisms that utilize a combination of Tyr-60, Arg-414, and His-59 to facilitate the proton movements between the oxygens at C-2 and C-1 within the *cis*-enediol intermediate and in the opening of the hemiacetal can be written. The proposed reaction mechanism for URI is different from that of metalloenzyme xylose isomerase since that enzyme catalyzes a hydride transfer mechanism rather than a proton transfer mechanism (*29*).

An alternative mechanism can be proposed in which Asp-412 abstracts the proton from the hydroxyl at C-5, which then abstracts a proton from C-2 to initiate the formation of the *cis*-enediol intermediate. The hydroxyl at C-5 is additionally activated through direct ligation to the bound zinc. These two variations are presented graphically in Figure 8. This latter mechanism is particularly attractive since it retains elements that are common to nearly all members of the amidohydrolase superfamily that have been interrogated mechanistically (*6*, *8*, *27*, *28*). The structural similarities in the active site of uronate isomerase with those members of the amidohydrolase superfamily nicely illustrate the evolutionary link between those members of the AHS that catalyze hydrolytic reactions and those that catalyze 1,2-proton transfers. A structural alignment of the active sites of Bh0493/D-glucuronate and dihydroorotase (DHO)/dihydroorotate (PDB entry 1j79) supports this proposition as illustrated in Figure 9. In this structural alignment, one of the C-6 carboxylate oxygens from D-glucuronate is positioned in nearly the same place as the carboxylate oxygen of the bridging carbamate functional group in DHO. These oxygen atoms interact directly with the α-metal (M_α) in their respective structures. Moreover, the C-5 oxygen of D-glucuronate is positioned in the same way as the nucleophilic hydroxide in DHO and is oriented to favor proton abstraction by Asp-412 at a distance of 2.9 Å. The C-5 hydroxyl is 2.0 Å from the hydrogen at C-2 of the bound substrate.

REFERENCES

1. Ashwell, G., Wahba, A. J., and Hickman, J. (1960) Uronic acid metabolism in bacteria. I. Purification and properties of uronic acid isomerases in *Escherichia coli*. *J. Biol. Chem. 235*, 1559–1565.
2. Wahba, A. J., Hickman, J., and Ashwell, G. (1960) Uronic acid metabolism in bacteria. III. Purification and properties of D-altronic acid and D-mannonic acid dehydrogenases in *Escherichia coli*. *J. Biol. Chem. 235*, 1566–1570.
3. Nguyen, T. T., Brown, S., Fedorov, A. A., Fedorov, E. V., Babbitt, P. C., Almo, S. C., and Raushel, F. M. (2008) At the periphery of the amidohydrolase superfamily: Bh0493 from *Bacillus halodurans* catalyzes the isomerization of D-galacturonate to D-tagaturonate. *Biochemistry 47*, 1194–1206.
4. Siebert, C. M., and Raushel, F. M. (2005) Structural and catalytic diversity within the amidohydrolase superfamily. *Biochemistry 44*, 6383–6391.
5. Holm, L., and Sander, C. (1997) An evolutionary treasure: Unification of a broad set of amidohydrolases related to urease. *Proteins 28*, 72–82.
6. Porter, T. N., Li, Y., and Raushel, F. M. (2004) Mechanism for the dihydroorotase reaction. *Biochemistry 43*, 16285–16292.
7. Benini, S., Rypniewski, W. R., Wilson, K. S., Miletti, S., Ciurli, S., and Mangani, S. (1999) A new proposal for urease mechanism based on the crystal structures of the native and inhibited enzyme from *Bacillus pasteurii*: Why urea hydrolysis costs two nickels. *Struct. Folding Des. 7*, 205–216.
8. Aubert, S. A., Li, Y., and Raushel, F. M. (2004) Mechanism for the hydrolysis of organophosphates by the bacterial phosphotriesterase. *Biochemistry 43*, 5707–5715.
9. Wilson, D. K., Rudolph, F. B., and Quiocho, F. A. (1991) Atomic structure of adenosine deaminase complexed with a transition state analog: Understanding catalysis and immunodeficiency mutation. *Science 252*, 1278–1284.
10. Ireton, G. C., McDermott, G., Black, M. E., and Stoddard, B. L. (2002) The structure of *Escherichia coli* cytosine deaminase. *J. Mol. Biol. 315*, 687–697.
11. Roy, J. E., and Roy, K. L. (1967) The mechanism and specificity of guanine deaminase. *Can. J. Biochem. 45*, 1263–1269.
12. Williams, L., Nguyen, T., Li, Y., Porter, T. N., and Raushel, F. M. (2006) Uronate isomerase: A nonhydrolytic member of the amidohydrolase superfamily with an ambivalent requirement for a divalent metal ion. *Biochemistry 45*, 7453–7462.
13. Sowden, J. C., and Oftedahl, M. L. (1961) Anhydridization of 1-deoxy-1-nitrohexitols. *J. Org. Chem. 26*, 1974–1977.
14. Dromowicz, M., and Koll, P. (1998) Synthesis of 2,6-anhydroaldonic acids from the corresponding anhydrodeoxynitroalditols (glycopyranosylnitromethanes) and their conversion into methyl esters, amides, and alditols. *Carbohydr. Res. 311*, 103–119.
15. Brouwer, A. C., and Kirsch, J. F. (1982) Investigation of diffusion-limited rates of chymotrypsin reactions by viscosity variation. *Biochemistry 21*, 1302–1307.
16. Maurice, M., and Bearne, S. L. (2002) Kinetics and thermodynamics of mandalate racemase catalysis. *Biochemistry 41*, 4048–4058.
17. Podlasek, C. A., Wu, J., Atripe, W. A., Bondo, P. B., and Serianni, A. S. (1995) [^{13}C]-Enriched methyl aldopyranosides: Structural interpretations of ^{13}C-^{1}H spin-coupling constants and ^{1}H chemical shifts. *J. Am. Chem. Soc. 117*, 8635–8644.
18. de Nooy, A. E. J., Besemer, A. C., and van Bekkum, H. (1995) Highly selective nitroxyl radical-mediated oxidation of primary alcohol groups in water-soluble glucans. *Carbohydr. Res. 269*, 89–98.
19. Bragd, P. L., van Bekkum, H., and Besemer, A. C. (2004) TEMPO-mediated oxidation of polysaccharides: Survey of methods and applications. *Top. Catal. 27*, 49–66.
20. Otwinowski, Z., and Minor, W. (1997) Processing of X-ray diffraction data collected in oscillation mode. In Methods in Enzymology (Carter, C. W. J., Sweet, R. M., Abelson, J. N., and Simon, M. I., Eds.) pp 307−326, Academic Pres, New York.
21. Long, F., Vagin, A., Young, P., and Murshudov, G. N. (2008) BALBES: A Molecular Replacement Pipeline. *Acta Crystallogr. D64*, 125–132.
22. Jones, A. T. (1985) Interactive computer graphics: FRODO. *Methods Enzymol. 115*, 157–171.

23. Brunger, A. T., Adams, P. D., Clore, G. M., DeLAno, W. L., Gros, P., Grosse-Kunstleve, R. W., Jiang, J. S., Kuszewski, J., Nilges, M., Pannu, N. S., Read, R. J., Rice, L. M., Simonson, T., and Warren, G. L. (1998) Crystallography & NMR system: A new software suite for macromolecular structure determination. *Acta Crystallogr. D54*, 905–921.
24. Lamzin, V. S., and Wilson, K. S. (1993) Automated refinement of protein models. *Acta Crystallogr. D49*, 129–147.
25. Collaborative Computational Project No. 4 (1994) The CCP4 suite: Programs for Protein Crystallography. *Acta Crystallogr. D50*, 760–763.
26. Hardy, L. W., and Kirsch, J. K. (1984) Diffusion-limited component of reactions catalyzed by *Bacillus cereus* β-lactamases I. *Biochemistry 23*, 1275–1282.
27. Hall, R. S., Xiang, D. F., Xu, C., and Raushel, F. M. (2007) N-Acetyl-D-glucosamine-6-phosphate deacetylase: Substrate activate via a single divalent metal ion. *Biochemistry 46*, 7942–7952.
28. Marti-Arbona, R., Fresquet, V., Thoden, J. B., Davis, M. L., Holden, H. M., and Raushel, F. M. (2005) Mechanism of the reaction catalyzed by isoaspartyl dipeptidase from *Escherichia coli*. *Biochemistry 44*, 7115–7124.
29. Allen, K. N., Lavie, A., Farber, G. K., Glasfeld, A., Petsko, G. A., and Ringe, D. (1994) Isotopic exchange plus substrate and inhibition kinetics of D-xylose isomerase do not support a proton-transfer mechanism. *Biochemistry 33*, 1481–1487.